Chem. Senses 34: 63–76, 2009
doi:10.1093/chemse/bjn051
Advance Access publication September 12, 2008

A Method for Generating Natural and User-Defined Sniffing Patterns in Anesthetized or Reduced Preparations

Man Ching Cheung[1], Ryan M. Carey[2] and Matt Wachowiak[1,2]

[1]Departments of Biology and [2]Biomedical Engineering, Boston University, 5 Cummington Street, Boston, MA 02215, USA

Correspondence should be sent to: Man Ching Cheung, Department of Biology, Boston University, Boston, MA 02215, USA. e-mail: mccheung@bu.edu

Abstract

Sniffing has long been thought to play a critical role in shaping neural responses to odorants at multiple levels of the nervous system. However, it has been difficult to systematically examine how particular parameters of sniffing behavior shape odorant-evoked activity, in large part because of the complexity of sniffing behavior and the difficulty in reproducing this behavior in an anesthetized or reduced preparation. Here we present a method for generating naturalistic sniffing patterns in such preparations. The method involves a nasal ventilator whose movement is controlled by an analog command voltage. The command signal may consist of intranasal pressure transients recorded from awake rats and mice or user-defined waveforms. This "sniff playback" device generates intranasal pressure and airflow transients in anesthetized animals that approximate those recorded from the awake animal and are reproducible across trials and across preparations. The device accurately reproduces command waveforms over an amplitude range of approximately 1 log unit and up to frequencies of approximately 12 Hz. Further, odorant-evoked neural activity imaged during sniff playback appears similar to that seen in awake animals. This method should prove useful in investigating how the parameters of odorant sampling shape neural responses in a variety of experimental settings.

Key words: active sensing, artificial sniffing, behavior, imaging, neural coding, respiration

Introduction

Olfactory sensation depends on the process of stimulus acquisition by the animal. For terrestrial vertebrates, inhalation of air into the nasal cavity is required for odorants to access the primary sensory neurons. This inhalation can occur in the course of baseline respiration or during the active sampling of odorants by specialized respiratory behavior (sniffing). The dependence of stimulus acquisition on respiration has profound consequences for olfactory system function. First, respiration imposes a strong temporal structure on the neural signal carried to the brain by olfactory receptor neurons (ORNs) (Spors et al. 2006; Verhagen et al. 2007). Second, there is strong evidence that changes in respiration have the potential to significantly alter the nature of neural responses, shaping their temporal organization, strength of activity, and even which neurons are activated (Mozell et al. 1991; Kent et al. 1996; Spors et al. 2006; Verhagen et al. 2007).

Sniffing is a rich and dynamic behavior, involving rapid changes in many parameters of respiration as a function of behavioral state and context (Welker 1964; Youngentob et al. 1987; Wesson et al. 2008b). Relatively little is known about how sniffing shapes odor coding and processing, however. It has long been hypothesized that sniffing can shape the neural representation of odorants (Mozell 1964, 1970; Mozell and Jagodowicz 1973), but these hypotheses have seldom been tested (but see Verhagen et al. 2007) during natural sniffing or at the level of the olfactory bulb (OB)—the first step in the central processing of odor information. Many previous studies have mimicked sniffing in anesthetized animals by drawing air through the nose using a vacuum—a process termed "artificial sniffing" or "artificial inhalation" (AI) in the literature (Macrides and Chorover 1972; Onoda and Mori 1980; Mair 1982; Harrison and Scott 1986; Sobel and Tank 1993). These studies have typically not varied the parameters of artificial sniffs, and—with a few exceptions (Macrides and Chorover 1972; Spors et al. 2006; Bathellier et al. 2008)—have been limited to only an inhalation phase at a fixed flow rate and interval. Other studies have investigated the effect of inhaled or exhaled flow rate on receptor neuron responses in reduced preparations (Kent et al. 1996; Scott-Johnson et al. 2000; Scott et al. 2006); these

studies have typically generated prolonged "static" flows that do not approximate the transient airflow changes that occur during sniffing.

Recordings of sniffing in awake, behaving animals (rats and mice, in particular) have shown that the intranasal pressure transients associated with each sniff (i.e., inspiration and exhalation) vary across many parameters and can do so on a cycle-by-cycle basis (Youngentob et al. 1987; Youngentob 2005; Kepecs et al. 2007; Wesson et al. 2008b). The most variable parameters (and those most directly relevant to airflow changes in the nasal cavity) are cycle frequency and both amplitude and duration of the inspiratory and expiratory phases of each sniff. An ideal way to investigate the role that these parameters play in shaping neuronal responses to odorants would be to accurately reproduce the intranasal pressure transients that occur during natural sniffing in reduced or anesthetized preparations and to parametrically vary specific parameters of a sniff while recording odorant-evoked activity. To our knowledge, however, this approach has not been attempted.

Here, in order to facilitate investigation of the relationship between sniffing and odor coding, we present a method for accurately reproducing natural waveforms in an anesthetized preparation or in any other reduced system. The method is based on an actuator-driven syringe device under the control of analog command waveforms that are derived either from previously recorded intranasal pressure transients or from user-defined signals. This "sniff playback" system is inexpensive, straightforward to assemble, and reliably reproduces intranasal airflow changes that occur during natural respiration or active sniffing. We also show that odorants presented using this system evoke neural responses that are similar to those seen during sniffing in the awake animal. We expect that this system will be useful in a variety of experimental paradigms aimed at understanding how sampling behavior shapes odor coding at multiple levels of the nervous system.

Materials and methods

Sniff playback system

Briefly, the sniff playback system uses a linear solenoid actuator to drive a syringe piston under the control of an analog voltage command pulse generated by a computer. The actuator is a Soft Shift Linear Solenoid (P/N: 192907-023, Johnson Electric, Vandalia, OH), whose piston is attached via a custom coupling to the piston of a standard glass syringe (Popper & Sons, Inc., New Hyde Park, NY). The syringe is mounted in an optics chuck (AOC1.0, Siskiyou Design, Grants Pass, OR) for stability, and both actuator and optics chuck are mounted on the same metal base plate. The actual syringe used depends on the animal preparation and is chosen to convert the full translational movement of the actuator to a suitable maximum working volume for rat or mouse: ≈1.5 ml for a 5-ml syringe (model #5118) and ≈0.5 ml for a 2-ml syringe (model #5108), respectively. The output of the syringe is connected via a short (~ 20 cm) length of polytetrafluoroethylene tubing (18 gauge) to the tracheotomy tube that enters the nasopharynx (described in Surgical procedures).

Analog command voltages ranging from 0 to 5 V are generated with custom software and output via an analog input/output PC board (PCI-6514, National Instruments, Austin, TX) in order to drive the solenoid. The interface between the computer output and the pump is a proportional driver (P/N: B5950-1000110, Canfield Connector, Youngstown, OH), which generates an output current proportional to the command signal, prevents overheating, and allows for additional adjustments to the response such as inertia compensation. Controls on the proportional driver are manually adjusted to optimize the sensitivity and frequency response of the system—this adjustment is only necessary on initial installation.

Digitized sniffing records acquired from awake animals (Verhagen et al. 2007; Wesson et al. 2008b) or user-defined synthetic traces are transformed into the command voltage signal using custom control software written in LabView (National Instruments). The control software allows for scaling the amplitude of the traces with a gain multiplier and for adjusting the baseline by adding an offset in order to use the full dynamic range of the actuator. The software also allows for triggered generation of command signals and for recording of the resulting pressure changes produced by playback. This software is freely available upon request.

Artificial inhalation

AI was produced as described previously (Wachowiak and Cohen 2001; Spors et al. 2006) by attaching a vacuum line to the sniff tube. Vacuum flow was controlled by a pinch valve, with the timing and duration of its open state controlled by a Master-8 stimulator (AMPI, Jerusalem, Israel). Vacuum strength was controlled by a manually adjusted flowmeter.

Recordings of intranasal pressure and airflow

Intranasal pressure transients produced by sniff playback were recorded via a cannula inserted into the dorsal recess, as described previously (Verhagen et al. 2007; Wesson et al. 2008b). Polyethylene tubing connected this cannula to a pressure sensor (P/N: 24PCBFA6G, Honeywell International, Inc., Morristown, NJ; range: ±5 psi, response time: 1 ms, sensitivity: 23 mV/psi, error: ±0.15% of span), the output of which was amplified 500× and low-pass filtered at 100 Hz using a PM-1000 transducer amplifier (CWE, Inc., Ardmore, PA). In the figures, inhalation (negative pressure) is shown as upward deflections. In some rats, we also recorded intranasal airflow transients using a grounded, stainless steel sheathed thermocouple (P/N: EMTSS-010G-12, OMEGA

Engineering, Inc., Stamford, CT; time constant: ~300 ms, sensitivity: 0.06 mV/1 °C, error: ±3%). The thermocouple recordings were done simultaneously with pressure measurements by implanting a T-connector into the dorsal recess to serve as the sniff cannula (see Figure 2). The thermocouple was inserted through the vertical arm of this connector and extended approximately 200 μm into the dorsal recess. The thermocouple signal was amplified 100× and low-pass filtered at 100 Hz with a BMA-931 AC/DC bioamplifier (CWE, Inc.).

Surgical procedures

Four adult female Long-Evans rats and 4 C57BL/6 mice (males and females) were used. The initial surgery for implanting the intranasal cannula was performed at least 2 days prior to the sniff playback experiment or dye loading. The implantation procedure was adapted from earlier studies (Verhagen et al. 2007; Wesson et al. 2008b). Animals were anesthetized with pentobarbital (50 mg/kg, intraperitoneally) and kept on a heating pad for the surgery. The head was secured in an appropriate head stereotax (David Kopf Instruments, Tujunga, CA). Before the sniff cannula was implanted, the skull was prepared by scraping with a scalpel blade and washing with H_2O_2. For rats, the intranasal cannula consisted of an 18 ga. stainless steel T-connector (Small Parts, Inc., Miramar, FL), with one arm trimmed to 2.4 mm from its base. This shortened end was inserted into the dorsal recess (from frontal–nasal fissure: 0 mm, from midline: 0.9 mm) and secured to the skull with 2 small skull screws (#000 × 3/32″) and dental cement. Wound margins were treated with a local anesthetic (1 mg/ml bupivicaine, Sigma-Aldrich, St Louis, MO) during surgery and with Betadine (Purdue Pharma LP, Stamford, CT) during recovery. The animal recovered while being kept warm on a heating pad, and after implantation, it was treated with the nonsteroid, anti-inflammatory pain relief agent Carprofen (5 mg/kg, Pfizer, New York, NY). For mice, the procedure was identical except that a 22-ga T-connector (Small Parts, Inc.) was used and was secured to the skull by dental cement. No anchor screws were used.

For the experimental sniff playback session, animals were anesthetized with pentobarbital and body temperature maintained using a heating pad. To allow for respiration independent of sniff playback, a double tracheotomy was performed as described previously (Wachowiak and Cohen 2001; Verhagen et al. 2007), and the breathing and sniff tubes were secured by tying silk suture around the trachea and closing the skin around the tubing and securing with VetBond (3M). All procedures were approved by the Boston University Institutional Animal Care and Use Committee.

Optical recordings

Sniff-evoked receptor input to the dorsal OB of rats and mice was imaged using calcium-sensitive dyes loaded into ORNs, as described previously (Wachowiak and Cohen 2001; Verhagen et al. 2007). Calcium Green-1 dextran (molecular weight = 10 000, $K_d \approx 376$ nM, Invitrogen, Carlsbad, CA) was used for all imaging experiments. Animals were held 3–8 days after loading before imaging. Optical signals were imaged through a thinned-bone optical window over one or both dorsal OBs. Signals were acquired using an Olympus BX51 illumination turret with a 150-W Xenon arc lamp (Opti-Quip, Highland Mills, NY), at 25% intensity, with the following filter set: excitation, 500 ± 25 nm; dichroic, 525 nm longpass; and emission, 530 longpass. Optical signals were recorded and digitized at 14-bit resolution using a back-illuminated CCD camera (NeuroCCD, SM-256, RedShirtImaging, Decatur, GA) with 256 × 256 pixel resolution at a 25-Hz frame rate. Data acquisition was performed with Neuroplex software (RedShirtImaging).

Data analysis

Pressure and thermocouple signals were digitized at 500 Hz (when acquired during sniff playback) or at 100 Hz (when acquired during imaging) and stored for offline analysis. Traces were further filtered as specified in the text to reduce noise. Comparison of command signals and pressure transients generated by sniff playback was performed as follows. For sinusoidal command signals (i.e., in the enclosed volume experiment), the mean peak-to-peak pressure amplitude was calculated for each trial. A different approach was used for sniff playback experiments involving irregular waveforms. First, cross-correlation between the command and the playback signals was used to identify the time lag between the 2 signals (typically, 23.7 ± 5.7 ms, $n = 93$ trials), and then the playback signal was shifted to align the 2 traces. A single scaling factor that minimized the difference between the 2 traces was then determined using the MatLab "polyfit" function; this scaling factor served as a relative measure of playback signal amplitude. Waveforms of command and playback signals were compared using standard Pearson's cross-correlation. All analyses were performed using custom MatLab (The MathWorks, Inc., Natick, MA) software.

Results

Intranasal pressure and flow measurements in awake rats and mice

Intranasal pressure changes associated with respiration were recorded from the dorsal recess of awake rats and mice via an implanted intranasal cannula (see Materials and methods). Recordings were made both from freely moving and head-fixed rats and from freely moving mice. Most of these recordings were made as part of previous studies (Verhagen et al. 2007; Wesson et al. 2008a; Wesson et al. 2008b). Sample traces of intranasal pressure transients are shown in Figure 1. As previously reported (Youngentob et al. 1987; Youngentob 2005; Verhagen et al. 2007; Wesson et al. 2008b), intranasal pressure recordings revealed respiration

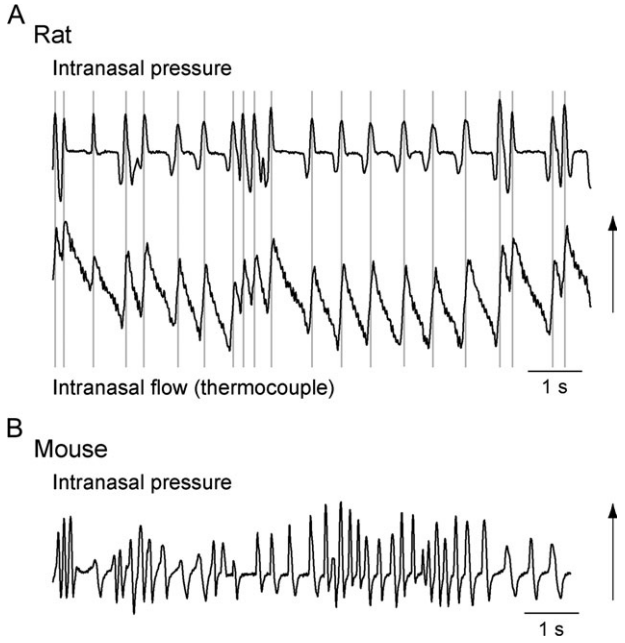

Figure 1 Complexity of sniffing behavior in awake rats and mice. **(A)** Intranasal pressure transients (top) recorded from the dorsal recess of a head-restrained rat. Individual respiratory cycles (sniffs) vary in amplitude, duration, waveform, and intersniff interval. Changes in intranasal airflow were recorded simultaneously with a thermocouple (bottom) and show rapid flow changes associated with each inspiration. Vertical lines indicate the pressure peak of each inhalation. Arrow indicates the direction of inhalation (negative pressure or thermocouple cooling). **(B)** Intranasal pressure transients recorded from the dorsal recess of an awake mouse. All traces were low-pass filtered (25 Hz).

waveforms that were highly varied and included changes in the amplitude, duration, waveform (relative degree of inhalation vs. exhalation), and frequency of the respiratory cycle. We did not distinguish between baseline respiration and odorant sampling (i.e., sniffing) in this study because we sought only to recreate any intranasal pressure transients that may occur in awake animals. For brevity, in subsequent text, we refer to all such transients as sniffs. Sniff waveforms appeared qualitatively similar in recordings from different animals; in general, only the absolute amplitude of the intranasal pressure signal varied from animal to animal—likely reflecting different degrees of patency of the nasal cavity and cannula implant.

In 3 rats, intranasal airflow transients were measured simultaneously with intranasal pressure by inserting a thermocouple probe through the barrel of the cannula (see Materials and methods). Thermocouple signals were time locked to each inhalation and showed a rapid onset associated with the influx of cooler air, followed by a slower decay that presumably reflected the gradual rewarming of the thermocouple probe (Figure 1). Thermocouple signals showed a range of different amplitudes, presumably reflecting different flow rates of inhaled air. These signals did not reliably report exhaled airflow because exhalation induces little or no temperature change at the probe tip. It was not possible to perform simultaneous pressure and thermocouple signals in awake mice due to the smaller size of the intranasal cannula.

Design and characterization of the playback system

To generate naturalistic patterns of respiratory behavior in anesthetized animals, we used the recorded intranasal pressure signals to control a sniff playback device. The device is described in detail in Materials and methods and consists of a solenoid-driven piston attached to the plunger of a syringe, the output of which was connected to a tube inserted via the trachea into the nasopharynx (the "sniff tube"). Control hardware allows the piston to be controlled by an analog command signal, which in this case consisted of intranasal pressure recordings obtained during awake sniffing (Verhagen et al. 2007). A schematic of this configuration is shown in Figure 2.

We first confirmed that it was possible to accurately reproduce recorded pressure signals in a closed system by connecting the syringe output to the same pressure sensor used in the original intranasal pressure recordings. After proper adjustment of the settings on the control hardware (see Materials and methods), we found that pressure transients recorded during sniffing in the awake animal could be reproduced with near-perfect fidelity. We determined that, for this particular actuator model and using a 5-ml syringe, the maximum piston movement translated into a 1.5-ml volume displacement. This volume falls within the range of tidal volumes measured in rat (0.9–2 ml), which have been shown to depend on a number of factors such as animal size, sex, health, and motor state (Walker et al. 1997; Seifert et al. 2000; Strohl and Thomas 2001).

We then characterized the frequency and gain response of the device using this closed system with a sinusoidal command waveform by connecting the 5-ml syringe to an enclosed reservoir and recorded the pressure within it. To examine the frequency response, we applied sinusoids at varying frequencies (0.2–20 Hz) at near-maximal gain (1.4 ml volume displacement) and correlated the command and measured pressure signals (Figure 3A). From 0.2 to 8 Hz, the correlation remained above 0.88, whereas the correlation decreased at higher frequencies, falling off dramatically above 12 Hz. To examine the gain response of the playback apparatus, we used a 2-Hz sinusoid as the command signal, scaled to different amplitudes via the control software (Figure 3B). The relationship between gain of the command and the amplitude of the resulting pressure signal was linear and the sinusoidal waveform was reproduced with high fidelity across a large-amplitude range, with significant deviations occurring only below 10% of the maximal gain. This initial characterization indicated that the sniff playback system is capable of reproducing time-varying signals at frequencies up to ~12 Hz and across an approximately 10-fold dynamic range.

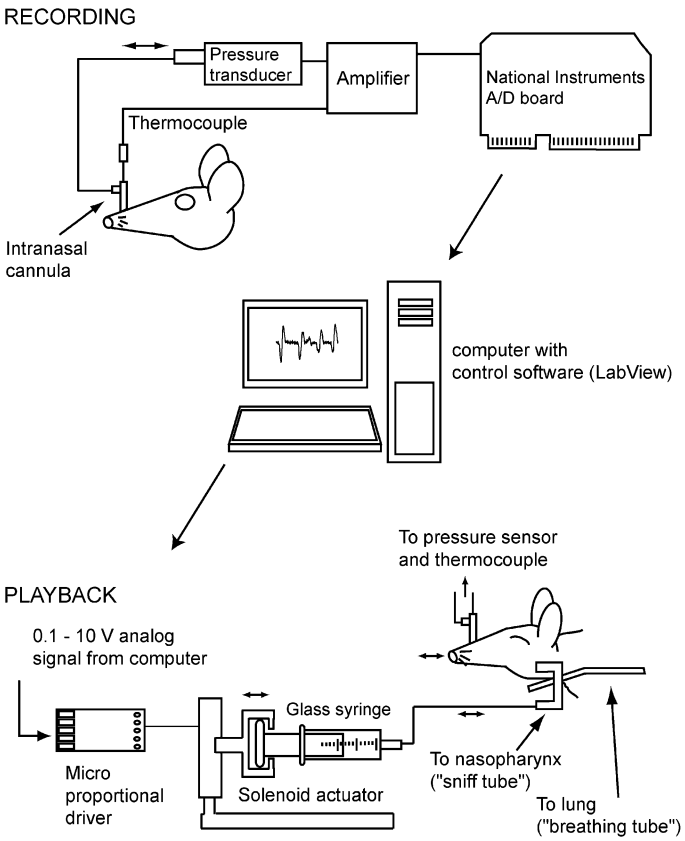

Figure 2 Schematic of the sniff playback system. For recording sniffing behavior, intranasal pressure and/or flow signals were recorded in awake animals using a chronically implanted intranasal cannula. Only the pressure signal was used to control sniff playback; the thermocouple signal was used for verification of playback fidelity. For sniff playback in the anesthetized animal, the pressure signal is sent as a scaled, analog voltage waveform to the artificial sniff hardware. The hardware consists of a microproportional driver that conditions the command signal and drives a linear solenoid actuator. The piston of the actuator is coupled to the plunger of a standard glass syringe. Teflon tubing connects the syringe to a polyethylene "sniff tube," which is directed through a tracheotomy toward the nasopharynx. A tube is also directed to the lungs to allow free breathing by the animal.

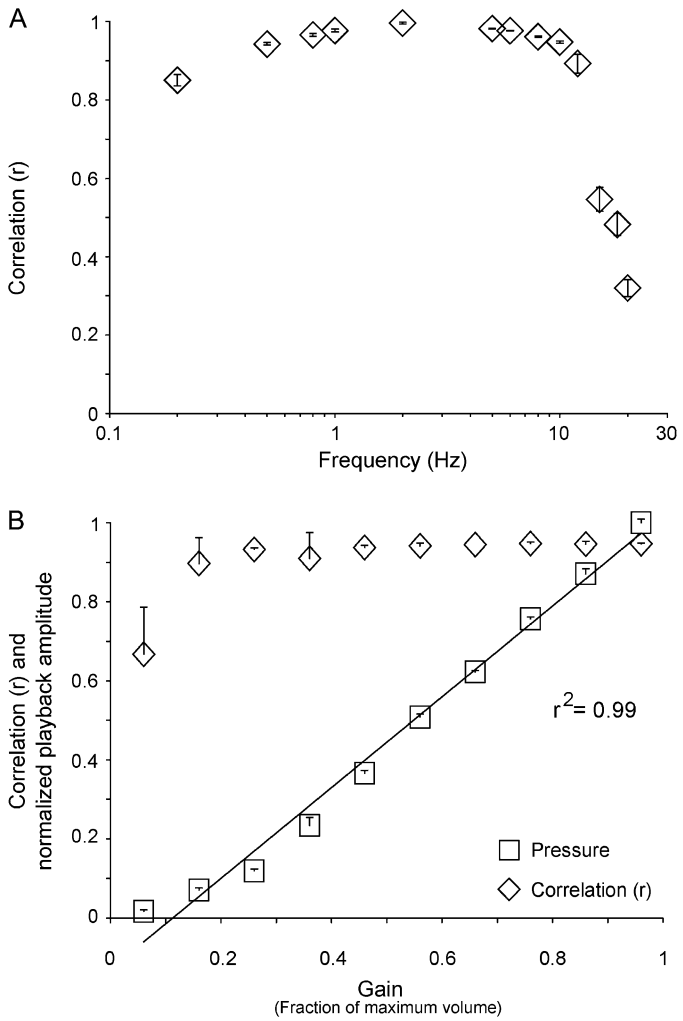

Figure 3 Frequency and gain response of the sniff playback system. **(A)** Correlation between a sinusoidal command and the resulting pressure signal is high for frequencies less than 12 Hz. The pressure signal was recorded from a closed reservoir, and all frequencies were played back at the same gain (96% of the 1.5-ml syringe maximum). Points show correlation coefficient (mean ± standard deviation [SD], n = 5 trials) between the pressure and the command signals. Correlations were performed on individual 10-s trials. **(B)** Amplitude and fidelity of playback pressure as a function of gain of the command signal. Pressure signals were recorded using a 2-Hz sinusoidal command signal. Gain is expressed as a fraction of the maximal syringe displacement (1.5 ml). Pressure "response" amplitudes were measured as the peak-to-peak value of the pressure signal (averaged across all cycles in a trial) and normalized to that of the highest gain (averaged across all trials). The average peak measurements (at least n = 3 trials) are shown (open triangles, mean ± SD). Many error bars are too small for display. Line shows linear fit to the data. Correlation between the command and the pressure signals was calculated and plotted (open squares) as in (A).

Playback of sniffing patterns in the anesthetized rat

Next, we tested whether the system could generate realistic pressure transients in the nasal cavity of an anesthetized rat. To test this, an intranasal cannula was implanted in the "test" rat and pressure signals recorded as they were for the awake recordings (Figure 4). Pressure traces showing low-frequency respiration seen in quiescent animals and those showing high-frequency (~6 Hz) exploratory sniffing were used in order to cover a range of different sniffing patterns.

Playback of both low- and high-frequency sniffing patterns generated pressure transients in the dorsal recess of the test animal that were similar to the original recordings (Figure 4A). The mean correlations between the playback pressure and the command signals were 0.91 ± 0.02 across 3 animals for predominantly low-frequency (~1 Hz) and a higher frequency (~6 Hz) exploratory sniffing, respectively. For this analysis, the playback pressure traces were averaged within each animal ($n \geq 4$ trials) before correlation. The fidelity of sniff playback from trial to trial was also high (Figure 4B), with a mean correlation coefficient of 0.97 ± 0.01 (n = 13

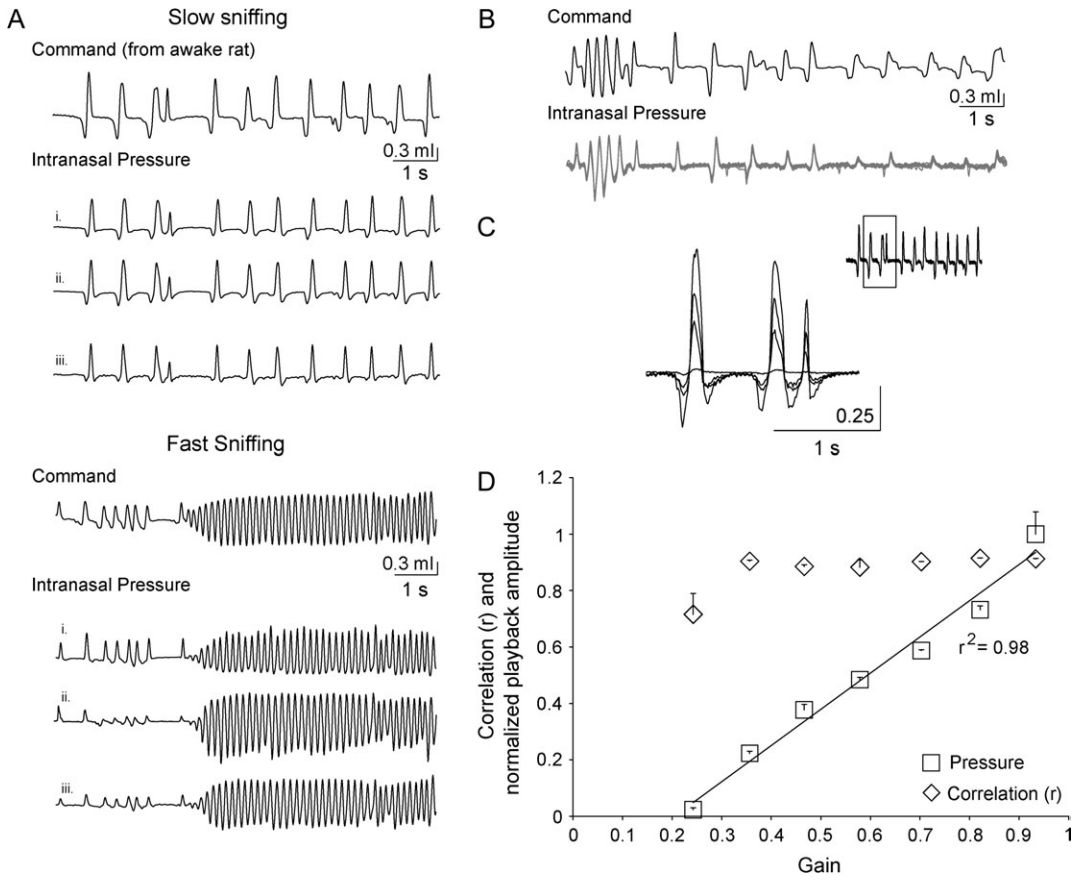

Figure 4 Sniffing recorded from awake rats can be reproduced in anesthetized preparations. **(A)** Comparison of sniff command and playback intranasal pressure signals recorded in different animals. The top set of traces shows low-frequency (slow) sniffing characteristic of quiescent rats (~1 Hz). The bottom set of traces includes high-frequency (fast) sniffing typical of active exploration (>6 Hz). "Command" trace shows the voltage signal used to drive the piston and syringe. The vertical bar indicates the scale of the command trace in terms of volume displacement (the scaling factor was calculated during device calibration). Intranasal pressure transients recorded in each of 3 anesthetized "test" rats during sniff playback are shown (i–iii). Each playback trace is the average of at least 4 trials and is normalized to its own maximum. All traces were low-pass filtered (25 Hz), with inhalation upwards. **(B)** Sniff playback is reproducible across trials. Top trace shows the command signal. Lower traces show intranasal pressure recordings from 13 individual trials (recorded from the same animal), normalized and overlaid. **(C)** Varying command signal gain changes playback pressure amplitude without affecting its waveform. The traces, from a single animal, are overlaid and show pressure transients generated at 24%, 47%, 73%, and 93% of maximal volume displacement. Inset shows the entire command trace from which these segments are taken. **(D)** Amplitude and fidelity of sniff playback pressure as a function of gain of the command signal. Gain is expressed as a fraction of the maximal syringe displacement (1.5 ml). Playback pressure amplitudes (open triangles) are shown using a scaling factor (arbitrary units) calculated for each trial (see Materials and methods). Each point (mean ± standard deviation) is the average of 3–6 trials from a single animal. Correlation (*r*) between the command and the playback signals (open squares) was calculated as in Figure 3. Error bars are present but may be too small for display. Traces in (A–C) were low-pass filtered (25 Hz), inhalation directed upwards.

trials, 1 animal, all pairwise comparisons) for the command pressure signal shown.

The absolute magnitude of the pressure change generated via sniff playback could be controlled by adjusting the gain of the command signal. Increasing the gain resulted in corresponding increases in the amplitude of the pressure transients generated in the test animal with little effect on waveform shape (Figure 4C). The relationship between command signal gain and playback pressure (see Materials and methods) was linear over a range of volume displacement from 0.3 to 1.4 ml (20–93% of maximal displacement) (Figure 4D; r^2 = 0.98). The correlation between the waveforms of the command and the playback signals also remained high across this range, falling somewhat at the lowest gain (Figure 4D). This relationship is similar to that observed in the ideal case of the closed system (Figure 3B). Thus, the sniff playback device is capable of reproducing pressure transients covering a variety of sniffing patterns and over a relatively wide dynamic range in anesthetized animals.

The ultimate goal of sniff playback is to generate intranasal airflow patterns that approximate those occurring during natural sniffing in the awake animal. To test this, we recorded airflow from the dorsal recess of test rats (n = 4) using a thermocouple. In 3 of these test rats, we recorded pressure and flow measurements simultaneously, using the same thermocouple probe and recording settings as we had used in

awake rats (see Material and methods). We compared thermocouple signals measured during playback of the same low- and high-frequency sniffing traces as used above with those measured in the awake rats. The thermocouple signal does not report absolute flow rate, only changes in intranasal temperature due to airflow. Comparisons were therefore made between the thermocouple signal waveforms rather than their absolute magnitudes.

During low-frequency sniffing, thermocouple signals measured during playback were similar to those seen in the awake animal, with each inhalation generating a distinct peak indicating an increase in inhaled flow rate (Figure 5A). Playback thermocouple signals did differ somewhat in waveform from those seen in the awake animal—primarily in showing a faster decay and also an apparent warming of the thermocouple probe during the exhalation phase of each sniff (seen as a deflection below baseline). This difference was most obvious during playback of high-frequency sniffing traces, in which each sniff generated a larger thermocouple transient during playback than seen in the awake animal (Figure 5A). The qualitative difference between thermocouple signals in awake animals versus during playback may be due to differences in intranasal temperature gradients in the different situations. Nonetheless, even during high-frequency sniffing, individual inhalation peaks in the thermocouple signal could be matched one-to-one in the awake and playback recordings (Figure 5A), indicating that in both cases each sniff generated a transient change in nasal airflow.

Taking the derivative of the command signal generates a waveform that is an estimate of the time-varying changes in airflow that should be produced by sniff playback. As shown in Figure 5B, the waveform of this derived flow rate command signal was similar to that actually measured via thermocouple during sniff playback of both low- and high-frequency sniffing traces. By scaling this signal to the maximal syringe displacement at a particular gain, one can also estimate the absolute changes in flow rate that are applied to the nasal cavity during playback (Figure 5B). Although potentially useful in matching sniff playback waveform amplitudes to airflow rates measured in vivo or used in prior studies (Youngentob et al. 1987; Sobel and Tank 1993; Scott-Johnson et al. 2000; Scott et al. 2006), we did not attempt to verify the accuracy with which sniff playback generated flow rate changes on an absolute scale.

One key advantage of sniff playback is the ability to reproduce relative changes in airflow that occur from sniff to sniff in the awake animal. We thus tested the degree to which changes in sniff amplitude yielded corresponding changes in inhaled flow rate as measured via thermocouple during playback. Figure 5C shows the peak amplitude of the thermocouple signal measured during sniff playback as a function of the peak instantaneous flow rate derived from the command. This relationship was measured in 4 rats using the low-frequency sniffing trace and varying the gain of the command pulse. Gain was varied so as to generate peak absolute flow rates that covered and slightly exceeded the range of flow rates measured in awake, actively sniffing rats (up to 20 ml/s) (Youngentob et al. 1987). Playback signals were normalized within each animal to correct for differences in absolute signal amplitude reflecting placement of the probe tip, nasal patency, or other factors (see Figure 5C, legend). For inhaled flow rates ranging from 5 to 20 ml/s, the relationship between predicted flow rate and measured thermocouple signal was linear ($r^2 \geq 0.88$ in all 4 animals). The slope of this relationship was also similar in different animals (Figure 5C). Thus, the sniff playback device is capable of generating graded changes in inhaled airflow that vary linearly and predictably with the amplitude of the command signal over a physiological range.

Playback of user-defined sniffing patterns

Another advantage of sniff playback is that it allows user-defined waveforms to be used to generate sniffing patterns in the anesthetized animal. These manipulations might range from the subtle—such as expanding or contracting a single respiration cycle—to the dramatic—such as creating an entirely synthetic sniffing pattern. Synthetic sniff traces would allow for a more controlled and systematic investigation of the influence of a particular parameter of sniffing behavior on evoked responses. To demonstrate this ability, we generated a synthetic sniff trace composed of a single sniff waveform recorded from a freely moving mouse repeated at different intervals (Figure 6A). We used a sniff recorded from a mouse for this demonstration because of its rapid rise and decay.

Because sniff frequency is a critical parameter shaping odor responses of ORNs (Spors et al. 2006; Verhagen et al. 2007), we generated synthetic sniff traces consisting of the single sniff repeated at frequencies ranging from 1 to 5 Hz (Figure 6A) and recorded intranasal airflow patterns via thermocouple in a test rat. We compared this method with thermocouple signals generated by "conventional" AI, which consisted of a square pulse of negative pressure, also generated at frequencies from 1 to 5 Hz (Figure 6B). A key difference between these methods is that AI consists solely of intermittent applications of vacuum that should generate no outward airflow, whereas the sniff playback method generates both negative and positive pressure transients that should lead to influx and efflux of air.

Example traces from this comparison are shown in Figure 6B. For these experiments, the vacuum strength was set to generate steady-state flows of 300 ml/min, in agreement with earlier studies using AI in rats (Harrison and Scott 1986; Scott-Johnson et al. 2000; Verhagen et al. 2007). Both intranasal pressure transients and thermocouple signals generated during sniff playback differed from that generated by AI. During AI, intranasal pressure changes were square shaped and showed no positive pressure (as expected),

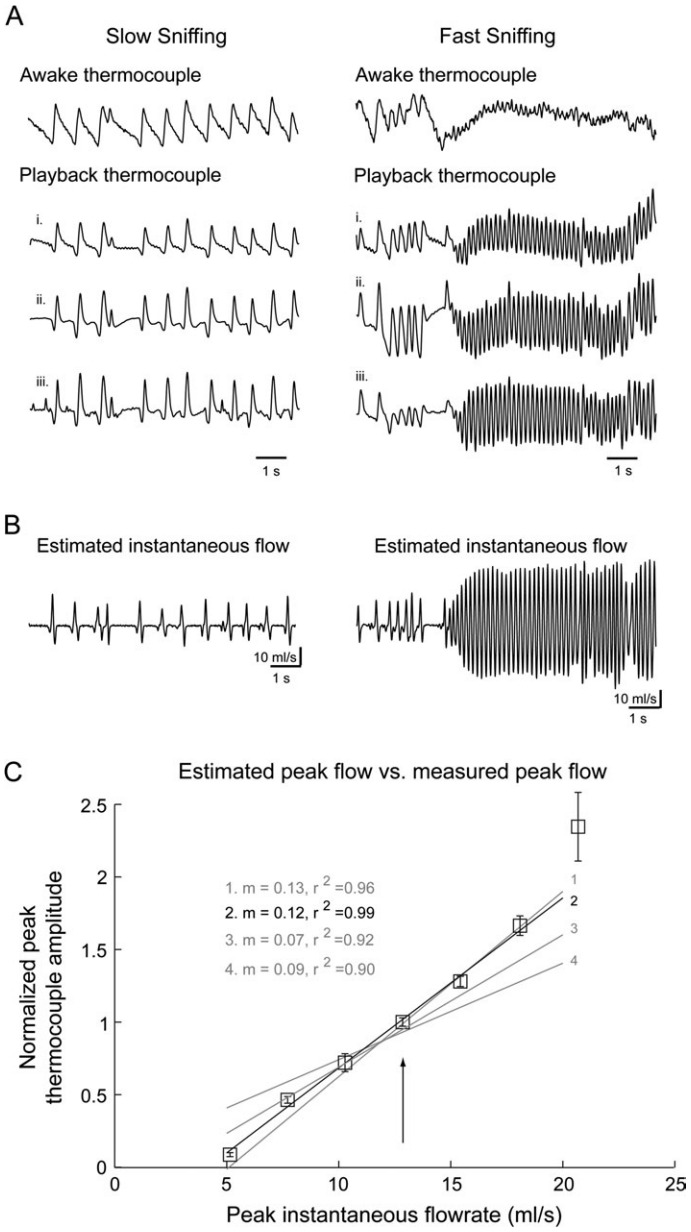

Figure 5 Intranasal airflow measured via thermocouple during sniff playback. **(A)** Comparison of thermocouple signals recorded in the awake rat (top traces) and during sniff playback for both slow (left) and fast (right) sniffing. The playback command signals were the same traces as in Figure 4A. Each playback trace (i–iii) is the averaged and normalized thermocouple signal (at least 4 trials) from a different animal. All traces are low-pass filtered (25 Hz) and normalized to their individual maxima. Upward deflections in the records indicate a temperature drop corresponding to inhalation. **(B)** Estimated instantaneous flow rate calculated by taking the numerical derivative of the command signal (shown in Figure 4A). **(C)** Peak thermocouple signal amplitudes scale linearly with instantaneous intranasal flow as command signal gain is varied. Instantaneous flow rate was calculated by taking the numerical derivative of the command trace. The mean peak value of all transients within a single thermocouple trace was averaged across trials and then plotted as a function of the peak instantaneous flow rate (n = 4 animals). To correct for differences in absolute thermocouple signal amplitudes across preparations, amplitudes were normalized to those measured at a playback gain common to all preparations (13 ml/s, arrow). Mean (± standard deviation) thermocouple values (squares) and the linear fit to these data (black line) are shown for one preparation (Preparation 2). The linear fits and their slopes (m) and regression coefficients (r^2) are shown for 3 other preparations (1, 3, and 4, gray lines).

whereas pressure transients evoked during playback consisted of brief spikes of negative and positive pressure (Figure 6B). The resulting thermocouple signals also differed, showing a slower rise and decay during AI than during playback and showing a clear outward flow of air during playback but not during AI. These differences were manifested most strongly at high frequencies. During AI at 5 Hz (100 ms duration), thermocouple signals showed attenuated phasic responses to each inhalation but maintained phasic responses during sniff playback at 5 Hz (Figure 6B). This effect is likely due to the repeated influx of air during high-frequency AI, as indicated by the tonic component of the thermocouple signal that emerges under these conditions (Figure 6B, left trace). In contrast, thermocouple signals show a rapid rewarming during the exhalation phase of sniff playback, even at high sniff frequencies. Thus, one significant difference between AI and sniff playback is the ability to modulate the "direction" of intranasal airflow; this distinction may have a significant impact on the dynamics of odorant-evoked responses in ORNs.

Sniff playback in the anesthetized mouse

We next tested whether the sniff playback device could be adapted for use in the anesthetized mouse. In theory, adjustment for playback in mice (or any other experimental model) simply requires use of a syringe of appropriate diameter so that the working range of the solenoid generates air displacements within the physiological range of the animal. For mice, we used a 2-ml syringe that generated a maximal displacement of 0.5 ml; this volume surpassed the tidal volume of a mouse, which is reported to range between 0.15 and 0.25 ml (Tankersley et al. 1997; Mitzner et al. 2001). We tested playback as we had done in rats by using intranasal pressure signals recorded from a freely moving mouse as the command signal and recording the resulting intranasal pressure transients in 2 anesthetized test mice (i and ii) via an intranasal cannula. We also found that it was possible to measure intranasal pressure transients without an intranasal cannula by simply placing a nose cone over the mouse's snout (lower trace, Figure 7A). Recording pressure at the external nares provides a simple method for assessing proper playback function without additional surgical procedures. As shown in Figure 7A, sniff waveforms were reliably reproduced during epochs of both low- (~2 Hz) and high frequency (~9 Hz) sniffing (r = 0.80 ± 0.01, n = 3 animals).

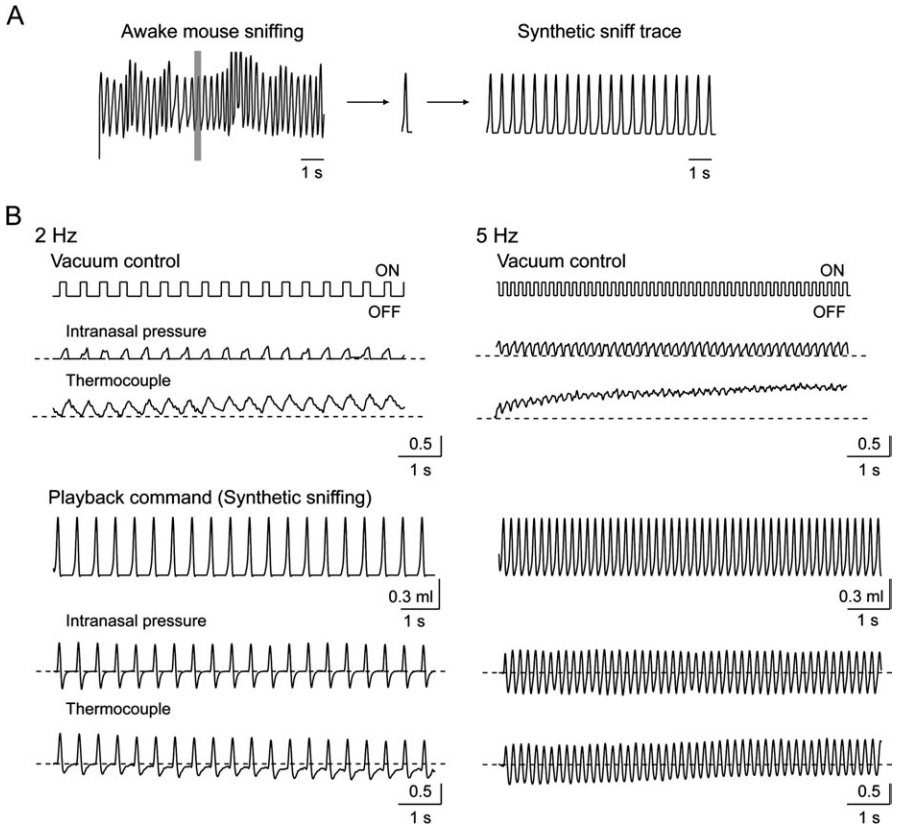

Figure 6 Playback of synthetic sniffing patterns derived from awake recordings. **(A)** Construction of a synthetic sniffing pattern from a single sniff recorded from an awake mouse. Gray box indicates the sniff that was extracted from the awake recording. The synthetic trace was constructed by repeating this sniff at regular intervals (right). The relative contribution of inhalation and exhalation components can be adjusted by applying an offset to this trace. **(B)** Intranasal pressure and airflow (via thermocouple) measured during conventional AI (300 ml/min, top traces) and playback of a synthetic sniff (lower traces) at 2 frequencies (2 and 5 Hz). Recordings were made in the same session under identical conditions. Acquisition began at the start of the sniff playback trace and approximately 100 ms after the start of AI. For 2- and 5-Hz AI and playback, pressure transients follow the application of each pulse or sniff, although for AI the pressure signals have a slower risetime and faster decay when compared with playback. At 2-Hz AI, thermocouple signals have a slower risetime and slower decay than those for synthetic sniffing and show no sign of exhalation. At 5 Hz, AI signals rapidly become dominated by a tonic cooling of the thermocouple, indicating continuous air influx with little modulation of flow. Playback of the synthetic sniff trace at 2 and 5 Hz generates both inhalation and exhalation flow transients, with only modest attenuation. Dotted horizontal line indicates baseline. Vertical bars indicate the same arbitrary scaling used for pressure and thermocouple traces.

As seen in rat, the relationship between the gain of the command pulse and the amplitude of the playback pressure signal in mice was linear over a tested range of 0.05–0.3 ml or 10–60% of maximal syringe displacement and 25–150% of a nominal mouse tidal volume of 0.20 ml (Figure 7B; $r^2 \geq 0.88$; $n = 3$ preparations, at least 3 trials per gain setting). The waveforms of the command and playback signals also remained similar at different gains (Figure 7C).

Verification of sniff playback fidelity by imaging receptor input to the OB

As a final test of the effectiveness of the sniff playback device in generating realistic patterns of odorant sampling, we imaged odorant-evoked receptor input to glomeruli of the dorsal OB during sniff playback, as described previously (Wachowiak and Cohen 2001; Spors et al. 2006; Verhagen et al. 2007). Figure 8A shows examples of sniffing records and the evoked signal imaged from ORN axon terminals in a glomerulus of an awake, head-fixed rat (left traces), compared with optical signals imaged from a different, anesthetized rat in which the same sniffing trace and odorant was used for sniff playback (right traces). Due to the differences in nasal resistance between animal preparations, an empirical adjustment of the gain of the command signal was sometimes necessary to facilitate effective stimulation of ORNs for both high- and low-amplitude sniffs. As long as the gain was adjusted to elicit odorant-evoked responses, sniff playback elicited odorant-evoked calcium signals that appeared remarkably similar to those measured in the awake animal, with distinct responses elicited by each inhalation. In this same animal, we imaged odorant-evoked responses during playback of the synthetic sniff trace at different frequencies (Figure 8B). At 2-Hz playback frequency, each sniff elicited a distinct response, whereas for 5 Hz, sniffing responses

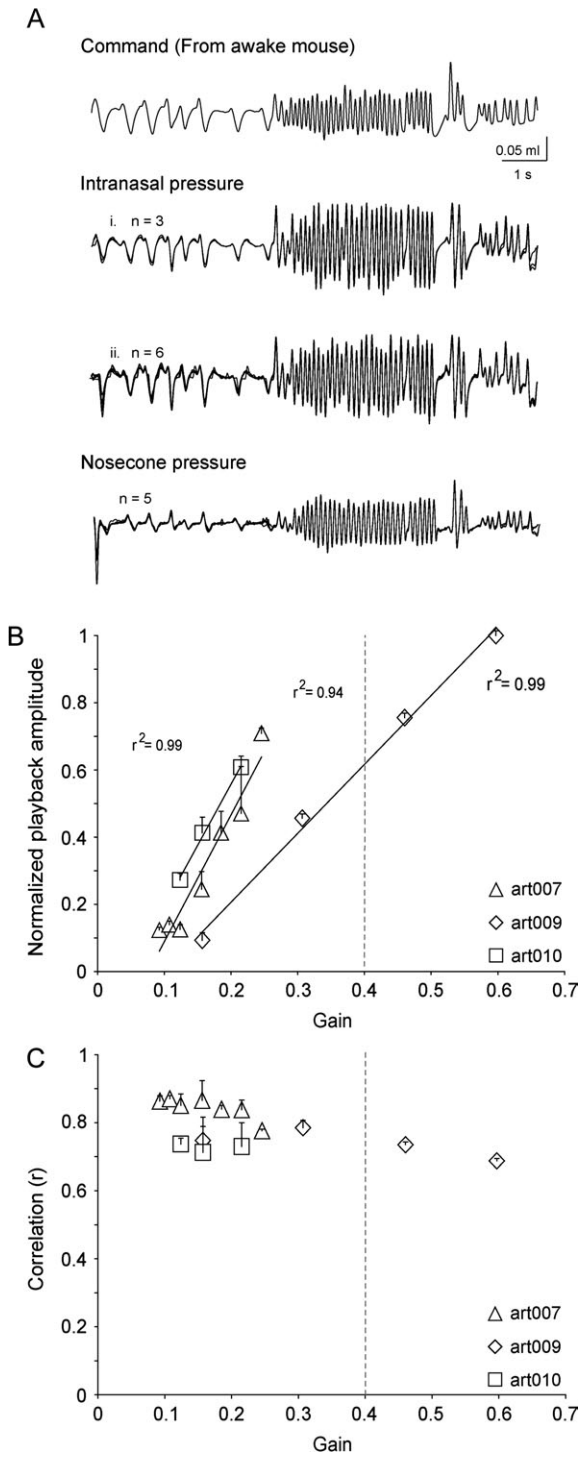

Figure 7 Sniff playback in the mouse. **(A)** Comparison of sniff command and playback signals recorded in an anesthetized mouse. The command signal (top) was recorded from a freely moving mouse as it sampled from an odor port. Intranasal pressure signals recorded during playback in 2 different mice are shown (i and ii), with traces from each animal normalized and overlaid. Pressure signals recorded from the external naris via a nose cone are also shown. **(B–C)** Amplitude (B) and correlation (C) of sniff playback pressure as a function of command gain. Gain is expressed as a fraction of the maximal syringe displacement (0.5 ml). Playback amplitude is expressed as an arbitrary scaling factor, as in Figure 4 (see Materials and methods). This scaling factor was not normalized across animals to illustrate differences in measurement sensitivity due to cannula placement, nasal patency, or other factors. In all animals, the relationship between gain and playback amplitude was linear. Points show the mean ± standard deviation [SD] of 3–6 trials per gain setting. The correlations (mean ± SD) between the intranasal and the command signal waveforms are plotted for the same trials. (C) Dashed vertical line marks approximate tidal volume of a mouse (0.2 ml).

became largely tonic, with little or no phasic response driven by each inhalation. This result is qualitatively similar to that seen in awake, freely sniffing rats (Verhagen et al. 2007).

Finally, we imaged odorant-evoked receptor input in an anesthetized mouse, using the sniff record recorded in a freely moving animal (Figure 8C). Odorant was presented for the length of the sniffing record. During the epoch with low sniffing frequencies, evoked responses were reliably driven by each sniff, whereas during the high-frequency sniffing epoch of the record, responses became tonic. There have been, to date, no recordings of receptor neuron input to the OB of awake, actively sniffing mice. However, the dynamics of the optical signal are consistent with those seen in anesthetized rat and mice for AI (Spors et al. 2006) and synthetic sniffing at these frequencies (Figure 8B).

Discussion

In the awake animal, respiratory behavior is complex and dynamic, and the waveforms of individual respiratory cycles can vary along multiple parameters (Youngentob et al. 1987; Wesson et al. 2008b). We have developed a sniff playback system for reproducing these waveforms and their resultant patterns of airflow through the nose, which is applicable to intact, anesthetized animals or to reduced preparations. The system is relatively inexpensive (total hardware cost, excluding computer, is ≈$800), straightforward to assemble, and enables the reliable reproduction of naturalistic sniffing patterns as well as generation of synthetic patterns that can be defined by the experimenter. This system represents an improvement over previous approaches to artificially controlling odorant sampling, which have typically relied on square pulses of inhalation or alternating inhalation and exhalation (Macrides and Chorover 1972; Mair 1982; Harrison and Scott 1986; Sobel and Tank 1993; Scott-Johnson et al. 2000; Wachowiak and Cohen 2001; Bathellier et al. 2008). This system should be useful in a number of different experimental settings.

Potential uses of the sniff playback system

One important application of the sniff playback system is in addressing the question of how odorant sampling behavior shapes the neural representation of odor information at different levels of the nervous system. For example, many previous studies have confirmed, using reduced preparations, that the direction and rate of airflow impact the spatial

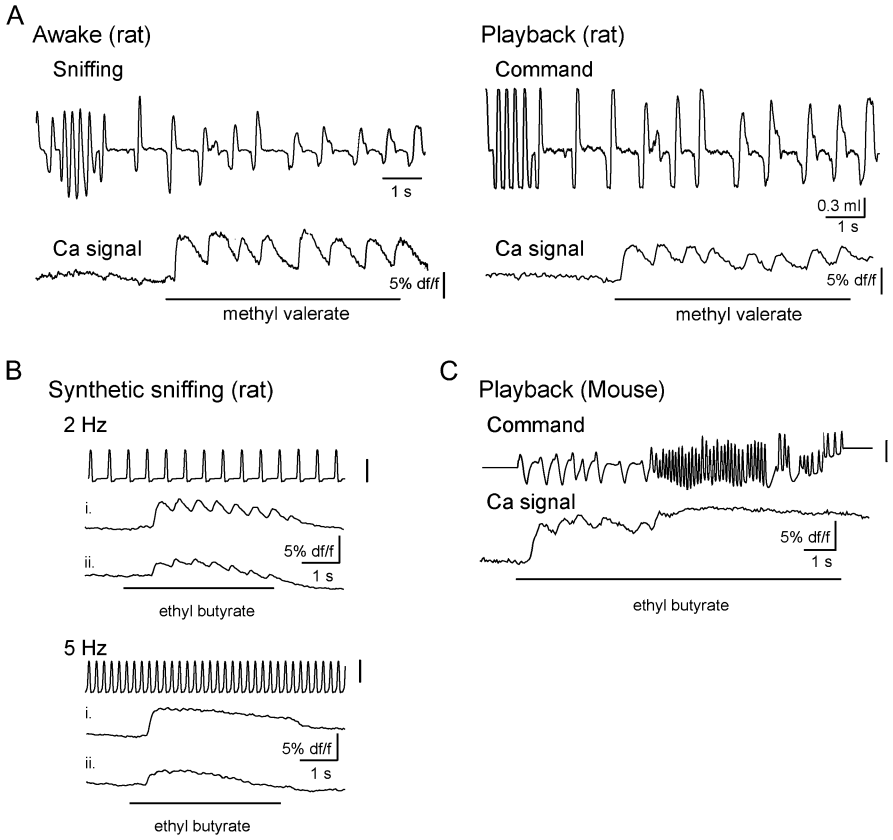

Figure 8 Olfactory receptor activation imaged from the OB using sniff playback in rat and mouse. **(A)** Left, Sniffing and odorant-evoked presynaptic calcium signals recorded from an awake, head-fixed rat. Right, Presynaptic calcium signals imaged in a second, anesthetized rat during playback of the awake sniffing trace. During playback, the timing of the odor pulse was matched to that of the awake trial. Sniffing and optical signal data are from (Verhagen et al. 2007). **(B)** Calcium signals imaged from the same rat (as in A) during playback of a synthetic sniff trace at 2 and 5 Hz (same command traces as in Figure 6). Responses are shown for 2 glomeruli (i and ii). The gain of the command signal was at rat tidal volume (1.4 ml). Vertical bar for command, 0.2 ml. **(C)** Calcium signal imaged in an anesthetized mouse during playback of an awake mouse sniffing pattern shown in Figure 7. Odorant was presented for the entire trial. Vertical bar for command, 0.2 ml. All odorants were presented at 1% saturated vapor.

distribution of odorant sorption across the olfactory epithelium, and this in turn shapes both spatial and temporal patterns of ORN activation (Mozell 1970; Hornung and Mozell 1977; Mozell et al. 1987; Kent et al. 1996; Scott 2006). However, these studies have used steady-state flows to characterize odorant sorption effects on receptor neuron responses; the extent to which these effects occur under conditions of natural sniffing has yet to be tested. Sniff playback, used in conjunction with acute surgical procedures such as exposure of the lateral olfactory epithelium for electroolfactogram recordings (Scott-Johnson et al. 2000) or imaging from the excised but intact nasal cavity (Kent et al. 1996), should allow odorant sorption effects to be tested across a range of realistic odorant sampling patterns. These effects could be tested using sniffs recorded in vivo or user-defined, synthetic waveforms that systematically vary in any number of parameters, including amplitude (peak flow rate), duration, or cycle length.

An important feature of the playback system is that invasive measurements of intranasal pressure are not required for playback to work effectively. In most of the experiments presented here, we did measure intranasal pressure during playback, but this was primarily to characterize the system and verify faithful reproduction of command pressure waveforms. Such monitoring is not necessary for routine use; we found that noninvasive verification of playback signals could be done in an anesthetized preparation at the external naris (Figure 7A). Even this level of monitoring is not necessary if one wishes to use sniff playback in a reduced preparation; instead, verification of pressure waveforms could be done in a closed "dummy" system prior to playback. Verifying accurate reproduction of the resulting airflow patterns is more difficult; we discuss the limitations of airflow measurements below.

Similarly, sniff playback will be useful in testing how odorant sampling behavior shapes odor representations at higher levels in the nervous system using in vivo, anesthetized preparations. For example, whether the sorption effects described at the level of the olfactory epithelium persist at the level of the OB, after receptor neurons have converged

onto OB glomeruli, has yet to be tested. As shown here (Figure 8), it is possible to record odorant-evoked activity from the OB (in this case, by imaging receptor inputs to OB glomeruli) during playback of awake sniffing behavior in an anesthetized preparation. The playback system allows these sniffing patterns to be reproduced reliably (e.g., when averaging responses across trials) and to be scaled along a given parameter (e.g., frequency or magnitude); this is not possible in awake or anesthetized, freely breathing preparations. Sniff playback should also be useful in examining the effect of sampling parameters on odorant-evoked activity in experiments requiring surgical approaches, more invasive recording methods (Cang and Isaacson 2003), or in vivo pharmacological manipulations (McGann et al. 2005).

Sniff playback will also be useful in separating the low-level effects of odorant sampling behavior on neural responses to odorants from those mediated by centrifugal modulation. For example, the spontaneous and odorant-evoked response properties of OB mitral/tufted cells change dramatically between awake and anesthetized animals (Rinberg et al. 2006) and also between resting states and high-frequency sniffing (Kay and Laurent 1999). These changes are likely mediated both by centrifugal modulation of OB network activity and by effects of sniffing behavior (e.g., sniff frequency) on ORN responses and postsynaptic processing (Verhagen et al. 2007; Pirez and Wachowiak 2008). Sniff playback in an anesthetized preparation should be useful in untangling the relative contribution of these processes to response properties of neurons in the OB and in piriform cortex.

Limitations of the sniff playback system

There are several limitations to the sniff playback system in replicating the full range of respiratory and sniffing behavior exhibited in awake animals. First, the dynamic range of pressure changes that the system is capable of reliably reproducing under ideal conditions (i.e., in a closed system) is approximately 10-fold, with generated pressures deviating from the command signal below ~10% of the maximal displacement. Performance was somewhat less when measured in a rat, with correlations between command and generated pressures falling modestly at 20% of maximal range. Nonetheless, this operating range covers the majority of natural variation in intranasal pressure transients observed during natural sniffing in rats and mice (e.g., see Figure 1) and so should be adequate for playback of most sniffing patterns. However, reproducing sniffing patterns that transition from low-amplitude, resting respiration (consisting primarily of inhalation) to higher frequency sniffing (consisting of large-amplitude inhalation and exhalation), such as that shown in Figure 4, may be difficult if the range of pressure changes for individual sniffs spans more than an order of magnitude.

Similarly, the frequency response of the playback system covers most—though not all—of the range of sniffing frequencies observed in mice and rats. The correlation between the command signal and the output of the playback system dropped for sinusoidal commands at frequencies above 12 Hz (i.e., Figure 3). Rats rarely, if ever, sniff at frequencies above 12 Hz (Welker 1964; Kepecs et al. 2007; Verhagen et al. 2007), although awake, freely moving mice sniff at frequencies above 12 Hz approximately 10% of the time (Wesson et al. 2008b).

Another limitation is that the faithfulness with which sniff playback is able to reproduce the detailed patterns of intranasal airflow that occur during sniffing is unclear, due to the difficulty in accurately monitoring airflow in either the awake or the anesthetized animal. The thermocouple approach used here can report influx of air into the nasal cavity, but does not reliably report efflux, and the dynamics of this signal can vary even under the same sniff-induced flow changes due to differences in thermocouple position placement and temperature differential between the nasal cavity and the outside air. For example, we observed differences in the thermocouple signal measured in the awake versus anesthetized animal, despite accurate reproduction of intranasal pressure changes. These differences could be due to technical issues such as the heating pad introducing a temperature gradient in the nasal cavity (such that air in the dorsal recess is cooler than that in the posterior nasapharynx) or differences in blood flow during anesthesia leading to less efficient warming of air as it enters the nasal cavity. It was thus difficult to compare thermocouple waveforms between awake and anesthetized animals and even—to some degree—between different animals.

Likewise, it is not possible to accurately measure or reliably reproduce the absolute flow rates that occur during natural sniffing using the sniff playback device, as the relationship between measured intranasal pressure and flow rate will vary depending on intranasal resistance, cannula resistance, and the pattern of airflow through the different nasal passageways. Absolute total flow rates can be "targeted" with sniff playback by adjusting the gain of the command signal and using the derivative of this signal and known syringe volumes to calculate flow velocity (see Figure 5B). However, we found that command signal gain ultimately needed to be adjusted empirically to a range effective in evoking odorant responses during sniff playback. Once this range is determined, however, relative changes in airflow—as measured by peak thermocouple signal amplitude—can be reliably reproduced in different animals and approximate those predicted from the command pressure signal generated during playback.

Comparison between AI and sniff playback

Most earlier studies that controlled odorant sampling have used square pulses of negative pressure applied to the nasopharynx to reproducibly draw odorant into the nasal cavity (Macrides and Chorover 1972; Mair 1982; Harrison and

Scott 1986; Sobel and Tank 1993; Scott-Johnson et al. 2000; Wachowiak and Cohen 2001). Our results suggest that there is indeed a difference between the dynamics and magnitude of intranasal airflow induced by AI and sniff playback (Figure 6). For example, AI caused changes in intranasal pressure and in airflow with slower dynamics than for sniff playback. One reason for the slower response of AI is that peak instantaneous flow rates generated during sniff playback (10 ml/s) were higher than the steady-state flow of AI (5 ml/s). Another reason is that sniff playback included an active exhalation or return to baseline pressure, rather than a passive switching of vacuum pressure and subsequent gradual decline in flow. Thus, sniff playback was able to generate cycle-coupled changes in the direction of intranasal airflow even at relatively high frequencies.

It is unclear what impact these differences may have on odorant-evoked neural activity. For example, we found that sniff playback of a synthetic sniff pattern at 5 Hz did not generate respiratory modulation of calcium signals imaged at the level of ORN inputs to the rat OB, and we observed similar results using playback of a high-frequency sniffing trace and imaging from the mouse OB (Figure 8). This result is consistent with an earlier study showing that, in the awake rat, receptor inputs to glomeruli fail to show respiratory modulation during high-frequency sniffing (Verhagen et al. 2007). Thus, at least for the parameter of sniff frequency, limitations in neuronal responsiveness (imposed, e.g., by transduction delays and adaptation effects) may be a more important determinant of response patterns than sampling behavior, obviating the need for carefully controlled sniff playback. Nonetheless, the ability to accurately and reproducibly control the parameters of odorant sampling seems a critical step in addressing this possibility. Sniff playback using the system described here provides a convenient means for doing so.

Funding

National Institute on Deafness and Other Communication Disorders, US National Institutes of Health (DC-06441 to M.W., DC-8116 to M.C.C. and M.W.).

Acknowledgements

We thank Daniel Wesson and Nicolás Pírez for their comments on the manuscript.

References

Bathellier B, Buhl DL, Accolla R, Carleton A. 2008. Dynamic ensemble odor coding in the mammalian olfactory bulb: sensory information at different timescales. Neuron. 57:586–598.

Cang J, Isaacson JS. 2003. In vivo whole-cell recording of odor-evoked synaptic transmission in the rat olfactory bulb. J Neurosci. 23: 4108–4116.

Harrison TA, Scott JW. 1986. Olfactory bulb responses to odor stimulation: analysis of response pattern and intensity relationships. J Neurophysiol. 56:1571–1589.

Hornung DE, Mozell MM. 1977. Factors influencing the differential sorption of odorant molecules across the olfactory mucosa. J Gen Physiol. 69: 343–361.

Kay LM, Laurent G. 1999. Odor- and context-dependent modulation of mitral cell activity in behaving rats. Nat Neurosci. 2:1003–1009.

Kent PF, Mozell MM, Murphy SJ, Hornung DE. 1996. The interaction of imposed and inherent olfactory mucosal activity patterns and their composite representation in a mammalian species using voltage-sensitive dyes. J Neurosci. 16:345–353.

Kepecs A, Uchida N, Mainen ZF. 2007. Rapid and precise control of sniffing during olfactory discrimination in rats. J Neurophysiol. 98: 205–213.

Macrides F, Chorover SL. 1972. Olfactory bulb units: activity correlated with inhalation cycles and odor quality. Science. 175:84–87.

Mair RG. 1982. Response properties of rat olfactory bulb neurones. J Physiol. 326:341–359.

McGann JP, Pírez N, Gainey MA, Muratore C, Elias AS, Wachowiak M. 2005. Odorant representations are modulated by intra- but not interglomerular presynaptic inhibition of olfactory sensory neurons. Neuron. 48: 1039–1053.

Mitzner W, Brown R, Lee W. 2001. In vivo measurement of lung volumes in mice. Physiol Genomics. 4:215–221.

Mozell MM. 1964. Evidence for sorption as a mechanism of the olfactory analysis of vapours. Nature. 203:1181–1182.

Mozell MM. 1970. Evidence for a chromatographic model of olfaction. J Gen Physiol. 56:46–63.

Mozell MM, Jagodowicz M. 1973. Chromatographic separation of odorants by the nose: retention times measured across in vivo olfactory mucosa. Science. 181:1247–1249.

Mozell MM, Kent PF, Murphy SJ. 1991. The effect of flow-rate upon the magnitude of the olfactory response differs for different odorants. Chem Senses. 16:631–649.

Mozell MM, Sheehe PR, Hornung DE, Kent PF, Youngentob SL, Murphy SJ. 1987. Imposed" and "inherent" mucosal activity patterns. Their composite representation of olfactory stimuli. J Gen Physiol. 90: 625–650.

Onoda N, Mori K. 1980. Depth distribution of temporal firing patterns in olfactory bulb related to air-intake cycles. J Neurophysiol. 44:29–39.

Pirez N, Wachowiak M. 2008. In vivo modulation of sensory input to the olfactory bulb by tonic and activity-dependent presynaptic inhibition of receptor neurons. J Neurosci. 28:6360–6371.

Rinberg D, Koulakov A, Gelperin A. 2006. Sparse odor coding in awake behaving mice. J Neurosci. 26:8857–8865.

Scott JW. 2006. Sniffing and spatiotemporal coding in olfaction. Chem Senses. 31:119–130.

Scott JW, Acevedo HP, Sherrill L. 2006. Effects of concentration and sniff flow rate on the rat electroolfactogram. Chem Senses. 31:581–593.

Scott-Johnson PE, Blakley D, Scott JW. 2000. Effects of air flow on rat electroolfactogram. Chem Senses. 25(25):761–768.

Seifert EL, Knowles J, Mortola JP. 2000. Continuous circadian measurements of ventilation in behaving adult rats. Respir Physiol. 120:179–183.

Sobel EC, Tank DW. 1993. Timing of odor stimulation does not alter patterning of olfactory bulb unit activity in freely breathing rats. J Neurophysiol. 69:1331–1337.

Spors H, Wachowiak M, Cohen LB, Friedrich RW. 2006. Temporal dynamics and latency patterns of receptor neuron input to the olfactory bulb. J Neurosci. 26:1247–1259.

Strohl KP, Thomas AJ. 2001. Ventilatory behavior and metabolism in two strains of obese rats. Respir Physiol. 124:85–93.

Tankersley CG, Fitzgerald RS, Levitt RC, Mitzner WA, Ewart SL, Kleeberger SR. 1997. Genetic control of differential baseline breathing pattern. J Appl Physiol. 82:874–881.

Verhagen JV, Wesson DW, Netoff TI, White JA, Wachowiak M. 2007. Sniffing controls an adaptive filter of sensory input to the olfactory bulb. Nat Neurosci. 10:631–639.

Wachowiak M, Cohen LB. 2001. Representation of odorants by receptor neuron input to the mouse olfactory bulb. Neuron. 32:723–735.

Walker JKL, Lawson BL, Jennings DB. 1997. Breath timing, volume and drive to breathe in conscious rats: comparative aspects. Respir Physiol. 107: 241–250.

Welker WI. 1964. Analysis of sniffing in the albino rat. Behavior. 22:223–244.

Wesson DW, Carey RM, Verhagen JV, Wachowiak M. 2008a. Rapid encoding and perception of novel odors in the rat. PLoS Biol. 6:e82.

Wesson DW, Donahou TN, Johnson MO, Wachowiak M. 2008b. Sniffing behavior of mice during performance in odor-guided tasks. Chem Senses. In press.

Youngentob SL. 2005. A method for the rapid automated assessment of olfactory function. Chem Senses. 30:219–229.

Youngentob SL, Mozell MM, Sheehe PR, Hornung DE. 1987. A quantitative analysis of sniffing strategies in rats performing odor discrimination tasks. Physiol Behav. 41:59–69.

Accepted August 6, 2008